Water Film Stiffness and Damping Analysis of Water Lubricated Bearings with Multiple Axial Grooves for Hydro Turbines

Dr.-Ing. Guojun (Gary) Ren, P. Eng.
Thordon Bearings Inc.
3225 Mainway, Burlington, On
Canada

Greg Auger. P. Eng.
Thordon Bearings Inc.
3225 Mainway, Burlington, on
Canada

Abstract

Water-lubricated bearings have found widespread application in vertical and horizontal hydro-turbines, primarily when used as main guide bearings. The end users can benefit from their simple installation, easy maintenance, and elimination of risk of oil leakage into the waterways. Turbine original equipment manufacturers can improve the turbine design by moving the bearing support point closer to the runner, thus reducing the cantilevered load on the shaft. Water-lubricated main guide bearings are conventionally designed with multi-axial grooves. These grooves are provided for the purpose of effectively cooling the bearing and flushing away abrasives, while maintaining a stable hydrodynamic lubricating film.

Questions often arise from hydro power engineers about the stiffness and damping characteristics of water lubricated guide bearings designed with multi-grooves. The main concern is their impact on rotor dynamic stability of the turbine, and comparison against oil lubricated bearing designs.

This paper mainly focuses on two aspects, the first is to provide a detailed method for calculating the stiffness and damping coefficients of water lubricated guide bearings with multi-grooves. This method is unique of this kind and provides a very practical approach in determining the stiffness and damping characteristics for bearings with multi-grooves. The second is to discuss the impact of the water lubricated bearing stiffness and damping on the overall stability of the rotating system. At the end, it provides a real case study where a water lubricated bearing has been designed and supplied for a modern turbine design.

1. Introduction

As known, water-lubricated main guide bearings are conventionally designed with multi-axial grooves. These grooves are provided for the purpose of effectively cooling the bearing and flushing away abrasives. However, due to the variety of groove design in terms of its number and size, a theoretical prediction of bearing performance in terms of load capacity, stiffness and damping characteristics is very difficult. Calculation methods for bearings with multi-axial grooves are rare to find in literatures. Current practice is that the load capacity, friction and wear characteristics of bearings are solely relying on experiments. Manufacturers provide testing results to their customers for products they supply. This paper introduces a method to calculate the stiffness and damping coefficients of water lubricated guide bearings with multi-axial grooves.

Before introducing the method, a brief review of available literature is useful to understand the development of this method. For plain bearings with no-grooves, literatures are abundant. In terms of steady operation, besides the classic solution of long bearing theory by Sommerfeld [10] and short bearing theory by DuBois and Ocvirk [13], there are several excellent analytical solutions for finite length bearings. A good solution for finite length bearing shall meet two criteria. Firstly, it shall provide the closest result as predicted by long bearing theory when bearing length to diameter ratio is large (greater than 2.0) and the closest result as predicted by short bearing theory when bearing length to diameter ratio is small (less than 0.5). Secondly, for an intermediate length to diameter ratio, it shall provide the closest result as predicted by long bearing theory when eccentricity ratio is high (close to unit) and closest result as predicted by short bearing theory when eccentricity ratio is low (less than 0.5). The finite length bearing theory by Childs and Moes [6] is one of the excellent solutions. Another good analytical solution is by Capone, et al [17]. Numerical solutions with using finite difference and finite element methods are abundant. The evaluation of them is not the focus of this paper. For bearings designed with multi-axial grooves, R.S. Pai and R. Pai [11] recently published a number of works on steady performance and dynamic stability of simple rotor. Recently, Ren [2] published a paper on calculation of water film thickness of water lubricated bearing with multi-axial grooves for steady state operation. The main idea is to use the analytical solutions of inclined slide bearing as building blocks to compose a circular bearing with multi-axial grooves. On stiffness and damping coefficients of non-grooved plain bearings, classical short bearing solution is the most popular one. The solution by Childs and Moes [3, 6] is strongly recommended for finite length bearings. For tilting pad journal bearings, the assembly method by Lund [14] is perhaps the most important

advancement during past 50 years. Nicholas et, al [15] provides a comprehensive overview on the development on this aspect. It needs to mention that above works are related to rigid surface bearings. For deformable surface bearings, the effect of surface deformation is considered. Lahmar et, al [16] provides a procedure to simultaneously evaluate both static and dynamic performance with small perturbation method. The same method is used by Lin and Hung [1] to evaluate the inclined slide bearings.

The method introduced in this paper is based on theoretical results from inclined slide bearings to evaluate the stiffness and damping coefficients of water film. Similar method was used by Lin and Hung [1] to evaluate the stiffness and damping characteristics of inclined slide bearings with exponential surface profile. The rigid surface assumption is continually applied.

For the calculation results to be useful, certain conditions for bearings have been applied. These shall be the same as for steady operation outlined in [2]. The ratio of bearing length to the width of stave must be greater than 3.0, the higher, the better. The bearing pressure shall be relatively low so that the surface deformation effect doesn't overwhelmingly change the result. There are two major difficulties on calculating stiffness and damping coefficients for water-lubricated main guide bearings with multi-axial grooves. One is the presence of grooves. And second is the surface deformation due to the relatively lower modulus of elasticity of materials which are commonly used for water-lubricated main guide bearings. Even though this paper doesn't consider the effect of elastic deformation of bearing surface in terms of elastohydrodynamic lubrication, the results do provide significant amount of information about the nature of bearing behavior. With using this information, it is possible for engineers and designers to adjust designed parameters, such as running clearance, number of grooves, allowed bearing pressure etc to optimize the bearing performance and prolong their operational life.

2. Stiffness and Damping evaluation of an inclined slider bearing

The idea used to evaluate the stiffness and damping coefficients is the same as evaluating the water film thickness for steady state operation [2]. A circular journal bearing with multi-axial grooves can be considered as an assembly of many simple inclined sliding pads (Figure-1). So the existing results for inclined sliding pads (Figure -2) can be used as building blocks to form a calculation method for circular journal bearings with multi-axial grooves. The implementation of this idea starts from evaluating the dynamic characteristics of the slide pad shown in Figure-2. The steady characteristics are already available. They are the load capacity and the location of load center.

A: Load capacity (force)

$$\frac{W_o \cdot h_{T0}^2}{\mu \cdot V \cdot B^2 \cdot L} = \frac{6 \cdot \left[(\eta+1)\cdot \ln \eta - 2\cdot(\eta-1)\right]}{(\eta-1)^2 \cdot (\eta+1)} \qquad (1)$$

B: Location of load center (distance)

$$\frac{x_C}{B} = \frac{\eta \cdot \left(\frac{\eta+2}{\eta-1}\right)\cdot \ln \eta - \frac{5}{2}\cdot(\eta-1) - 3}{(\eta+1)\cdot \ln \eta - 2(\eta-1)} \qquad (2)$$

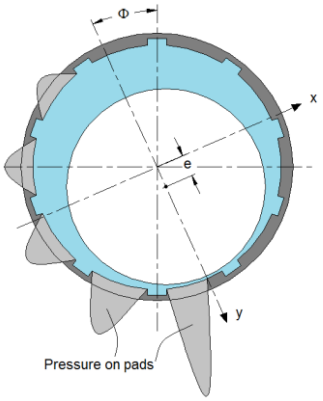

Figure-1: A grooved circular Bearing is an array of sliding pads

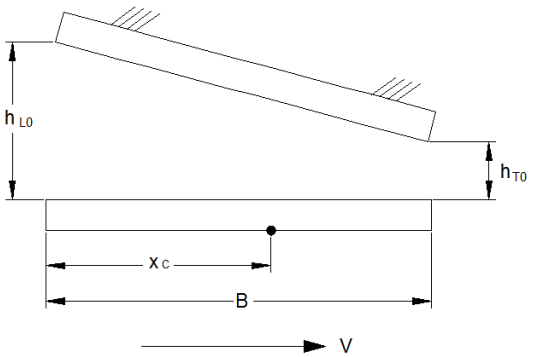

Figure-2: Infinite length inclined sliding pad

In equation (1) and (2)

B – Width of each pad
L – Bearing length, this is the length of pad.
μ - Viscosity of lubricant, for water it is a constant
V- Surface velocity of shaft
$\eta = h_{L0} / h_{T0}$ (Ratio of film thickness at leading edge to trailing edge)
W_o - Bearing force

It is noticed that the right side of equation (1) and (2) is only a function of the ratio of film thickness at leading to the film thickness at trailing edge. For the purpose of evaluating stiffness and damping, the film thickness at leading and trailing edges is considered as a function of time. This is shown in Figure -3 below:

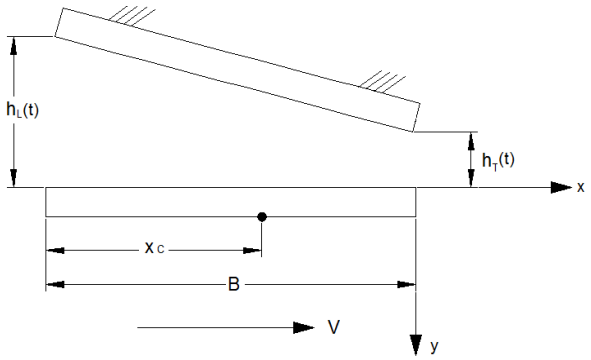

Figure-3: Infinite length inclined sliding pad considering dynamic motion

Moreover, even the film thickness at both leading and trailing edges is function of time, the ratio is assumed not changed with time. This will simplify the analysis significantly [1]. Same as for steady operation, it requires the length to width ratio (L/B) at least at 3.0. According to Figure-3, the film thickness can be expressed as

$$h(x,t) = h_T(t) \cdot \left[1 - (\eta - 1) \cdot \frac{x}{B}\right] \qquad (-B < x < 0, \text{ see Figure-3}) \qquad (3)$$

Introducing non-dimensional variables and parameters defined as following.

$$x^* = \frac{x}{B}; \quad \tau = \frac{V \cdot t}{B}; \quad h_T^* = \frac{h_T(t)}{h_{T0}}; \quad h^* = h_T^* \cdot \left[1 - (\eta - 1) \cdot x^*\right]; \quad p^* = \frac{p \cdot h_{T0}^2}{\mu \cdot V \cdot B} \qquad (4)$$

The unknown parameters in equation (4) are:

h_{T0} – The minimum water film thickness as trailing edge of bearing operating under steady state
p – Pressure over the pad
t- Time

The Reynolds Equation taking into consideration on squeezing film action is as following.

$$\frac{\partial}{\partial x}\left(h^3 \cdot \frac{\partial p}{\partial x}\right) = 6 \cdot \mu \cdot V \cdot \frac{\partial h}{\partial x} + 12\mu \cdot \frac{\partial h}{\partial t} \qquad (5)$$

Insert non-dimensional variables (4) into equation (5), the Reynolds equations non-dimensional form is

$$\frac{\partial}{\partial x^*}\left(h^{*3} \cdot \frac{\partial p^*}{\partial x^*}\right) = 6 \cdot \frac{\partial h^*}{\partial x^*} + 12 \cdot \frac{\partial h^*}{\partial \tau} \qquad (6)$$

Small perturbation method means a solution of equation (6) not far from the steady state solution with a linearization approach. This is to find a solution such as

$$p^* = p_o^* + p_1^* \cdot \delta \cdot e^{i \cdot \tau} \quad (7)$$

$$h_T^* = 1 + \delta \cdot e^{i \cdot \tau} \quad (8)$$

Here:

p_0^* - Non-dimensional pressure under steady operation

p_1^* - Perturbation amplitude of a pressure on top of the pressure under steady operation

δ - A small perturbation – a small number much less than 1.0. Its physical meaning is the ratio of amplitude change of film thickness to the minimum film thickness under steady operation. Insert expression (7) and (8) into (6), the dynamic part of pressure p_1^* will fulfill following equation

$$\frac{\partial}{\partial x^*}\left(\left[1-(\eta-1)\cdot x^*\right]^3 \cdot \frac{\partial p_1^*}{\partial x^*}\right) = 12\cdot(\eta-1) + 12\cdot\left[1-(\eta-1)\cdot x^*\right]\cdot i \quad (9)$$

The boundary condition for equation (9) is

$p_1^* = 0$ for $x^* = 0$ and $x^* = -1$

A non-dimensional force result from the dynamic pressure p_1^* can be obtained by integrating this pressure over the entire width of pad.

$$\frac{W_1 \cdot h_{T0}^2}{\mu \cdot V \cdot B^2 \cdot L} = \int_{-1}^{0} p_1^* \cdot dx^* \quad (10)$$

Since p_1^* is a complex function, therefore, integration is also a complex function. After evaluation of equation (10) by solving Reynolds equation (9), the end result becomes

$$\frac{W_1 \cdot h_{T0}^2}{\mu \cdot V \cdot B^2 \cdot L} = \left[K(\eta) + i \cdot C(\eta)\right] \quad (11)$$

Where:

$$K(\eta) = 6 \cdot \frac{2 \cdot \eta \cdot \ln\eta - \eta + 1}{\eta \cdot (\eta-1)^2} - \frac{6}{\eta \cdot (\eta+1)} + \frac{12}{1-\eta^2} \quad (12)$$

$$C(\eta) = -6 \cdot \frac{\eta \cdot \ln\eta - \eta + 1}{(\eta-1)^3} + 6\frac{\eta \cdot \ln\eta}{(\eta^2-1)\cdot(\eta-1)} \quad (13)$$

The non-dimensional function on the right side of equation (11) is a complex function. The real part K (η) is stiffness function and the imagine part C (η) is damping function.

Looking back at equation (7), the dimensional bearing force (load capacity) under dynamic load will be

$$W = W_0 + \frac{\mu \cdot V \cdot B^2 \cdot L}{h_{T0}^2}\left[K(\eta) + i \cdot C(\eta)\right] \cdot \delta \cdot e^{i \cdot \tau} \quad (14)$$

Where:

W – The total supporting force that the slide bearing creates

W_o – The load capacity under steady operation (equation (1))

The variable δ in equation was introduced only instrumental at very beginning. However, if looking at equation (8) carefully, it is realized that δ is a relative change of amplitude of film thickness. This leads to

$$\delta \cdot e^{i\cdot\tau} = \frac{\Delta h_T(\tau)}{h_{T0}}; \quad i \cdot \delta \cdot e^{i\cdot\tau} = \frac{\Delta \dot{h}_T(\tau)}{h_{T0}} \tag{15}$$

Where:

$\Delta h_T(\tau)$ – Dynamic deflection at trailing edge

$\Delta \dot{h}_T(\tau) = \frac{B}{V} \cdot \Delta \dot{h}_T(t)$ - The squeeze velocity of the pad

Now equation (14) becomes:

$$W = W_0 + \frac{\mu \cdot V \cdot B^2 \cdot L}{h_{T0}^3} \cdot K(\eta) \cdot \Delta h_T(t) + \frac{\mu \cdot B^3 \cdot L}{h_{T0}^3} \cdot C(\eta) \cdot \Delta \dot{h}_T(t) \tag{16}$$

Equation (16) is the pad force under dynamic motion. It is the fundamental relationship between the pad force and pad displacement and squeeze velocity. It is going to be used to build circular bearing with grooves.

3. Assembly Procedure

The assembly procedure is similar to the situation under steady operation [2]. The first step is to define the location angles of each pad relative to a rotating co-ordinate frame R-ϕ. Figure-4 shows a journal bearing with multi-axial grooves under a steady operational condition. By given load and shaft speed, the shaft center is offset from bearing center with an eccentricity of "e". The connecting line between bearing center and shaft center is in-line with "R"-axis of the moving coordinate system R-ϕ. Assuming the bearing is fixed in position and the load is vertical as shown on the figure, the R-ϕ coordinate system has an attitude angle "Φ" with respect to the loading direction, namely, the y-axis. The attitude angle changes depending on load, shaft speed and groove numbers.

A second co-ordinate frame x-y is defined in line with load direction. In this system, y-axis is in load direction and x-axis is perpendicular to the load direction.

In Figure-4, the R-axis divides the entire bearing into two equal halves. All pads underneath R-axis (in the sense if the Figure) have convergent angles in shaft rotating direction and therefore are able to create hydrodynamic lifting forces. All pads above R-axis have divergent angles in shaft rotating direction and are therefore not able to create hydrodynamic lifting forces. In theory, the divergent bearing half could create a vacuum and therefore a negative pressure. However, since in practice, almost in all the cases, outside source of lubricant will be supplied to the bearing grooves, the divergent half will not create a negative pressure, but keep the same level of pressure as supplied lubricant as in grooves. It is therefore acceptable to assume the pressure on that half of bearing as zero. This assumption is actually corresponding to half Sommerfeld or Gumbel boundary condition.

Since the bearing is assumed to be fixed on ground, all angles (α_{Li} , α_{Ti} = 1, 2, 3 … N/2) defining the positions of grooves will change with attitude angle which is an unknown parameter. One set of groove location angles only defines a particular equilibrium of steady operation. For calculation purpose, a set of "floating numbers" are assigned to the pads underneath the R-axis. As a rule, no matter how the attitude angle to change, it is always the first convergent pad underneath R-axis at the smallest water film location is called number "1". Other pads are enumerated clockwise with number 2, 3, 4 etc in sequence.

After having defined the pad location angles, the film thickness ratio of leading to trailing edge under steady operation condition is

$$\eta_i = \frac{1 + \varepsilon \cdot \cos \alpha_{L,i}}{1 + \varepsilon \cdot \cos \alpha_{T,i}} \qquad (i = 1, 2 \ldots N/2) \tag{17}$$

The film thickness at any leading and trailing edge is

$h_{T0,i} = c \cdot (1 + \varepsilon \cdot \cos \alpha_{T,i})$, $\qquad (i = 1, 2 \ldots N/2)$ (18)

$$h_{L0,i} = c \cdot (1 + \varepsilon \cdot \cos \alpha_{L,i}) \,, \qquad (i = 1, 2 \ldots N/2) \tag{19}$$

Where:
ε - Eccentricity ratio of the entire bearing (ε = e/c)
c – Radial clearance of entire bearing

The second step is to calculate the force contribution of each pad to support the bearing load. Figure -5 illustrates the supporting force from a pad with location angles α_{Li} , α_{Ti} . Considering (18) and (19), the force by this pad can be calculated with using equation (16) obtained from previous section.

$$W_i = W_{0i} + \frac{c_1 \cdot K(\eta_i)}{(1 + \varepsilon \cdot \cos \alpha_{Ti})^3} \cdot \Delta h_{Ti}(t) + \frac{c_2 \cdot C(\eta_i)}{(1 + \varepsilon \cdot \cos \alpha_{Ti})^3} \cdot \Delta \dot{h}_{Ti}(t) \tag{20}$$

With $c_1 = \dfrac{\mu \cdot V \cdot B^2 \cdot L}{c^3}$; $\quad c_2 = \dfrac{\mu \cdot B^3 \cdot L}{c^3}$

All terms in equation (20) are referred to pad number 'i'.

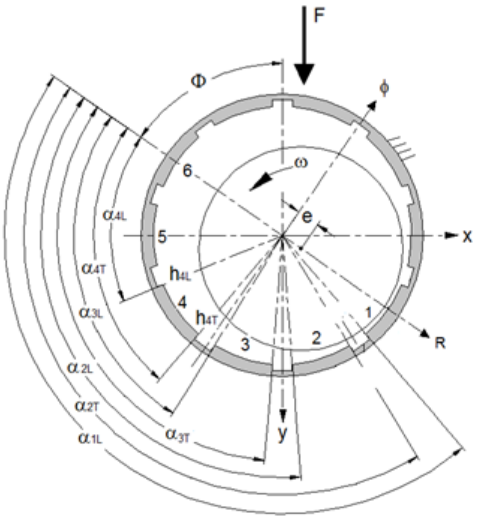

Figure-4: Pad Location Angles

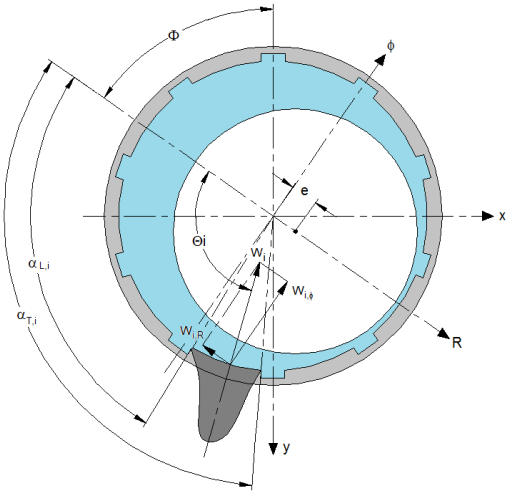

Figure-5: Pad Force

In Figure-5, the pad load is considered to be in direction perpendicular to bearing surface. The projection of bearing load to R-ϕ co-ordinate system is

$$W_{i,r} = -\left(W_{0i} + \frac{c_1 \cdot K(\eta_i)}{(1 + \varepsilon \cdot \cos \alpha_{Ti})^3} \cdot \Delta h_{Ti}(t) + \frac{c_2 \cdot C(\eta_i)}{(1 + \varepsilon \cdot \cos \alpha_{Ti})^3} \cdot \Delta \dot{h}_{Ti}(t) \right) \cdot \cos(\pi - \Theta_i) \tag{21}$$

$$W_{i,\phi} = \left(W_{0i} + \frac{c_1 \cdot K(\eta_i)}{(1 + \varepsilon \cdot \cos \alpha_{Ti})^3} \cdot \Delta h_{Ti}(t) + \frac{c_2 \cdot C(\eta_i)}{(1 + \varepsilon \cdot \cos \alpha_{Ti})^3} \cdot \Delta \dot{h}_{Ti}(t) \right) \cdot \sin(\pi - \Theta_i) \tag{22}$$

For the entire circular bearing, the dynamic part of pad force is only caused by a very small change of bearing eccentricity Δe and attitude angle ΔΦ, the minimum film thickness at trailing edge can be related to these small eccentricity and attitude angle change therefore as follows

$$\Delta h_{Ti} = \cos \alpha_{Ti} \cdot \Delta e + \sin \alpha_{Ti} \cdot e \cdot \Delta \Phi \tag{23}$$

The same can be applied to the pad velocity. However, since the velocity is referred to entire pad, not just the trailing edge, therefore the velocity becomes:

$$\Delta \dot{h}_{Ti} = \cos(\pi - \Theta_i) \cdot \Delta \dot{e} + \sin(\pi - \Theta_i) \cdot e \cdot \Delta \dot{\Phi} \qquad (24)$$

e – Eccentricity in equation (23) and (24)

$$\Theta_i = \xi_i \cdot \alpha_{Ti} + (1 - \xi_i) \cdot \alpha_{Li}$$

$$\xi_i = \frac{\eta_i \cdot \left(\frac{\eta_i + 2}{\eta_i - 1} \right) \cdot \ln \eta_i - \frac{5}{2} \cdot (\eta_i - 1) - 3}{(\eta_i + 1) \cdot \ln \eta_i - 2(\eta_i - 1)} \qquad (i = 1, 2, 3 \ldots N/2)$$

With using equation (22) to (24), the load capacity, stiffness coefficients and damping coefficients can be evaluated.

4. Steady Operation and Sommerfeld Number

Reference [2] provides a procedure to calculate the load capacity and water film under steady operational condition. The non-dimensional load capacity of bearing was determined as follows

$$W_{0\phi,i} = \frac{\Pi(\eta_i)}{(1 + \varepsilon \cdot \cos \alpha_{Ti})^2} \cdot \sin\{\pi - \Theta_i\} \qquad (25)$$

$$W_{0r,i} = \frac{\Pi(\eta_i)}{(1 + \varepsilon \cdot \cos \alpha_{Ti})^2} \cdot \cos\{\pi - \Theta_i\} \qquad (26)$$

Where:

$$\Pi(\eta_i) = \frac{6 \cdot [(\eta_i + 1) \cdot \ln \eta_i - 2 \cdot (\eta_i - 1)]}{(\eta_i - 1)^2 \cdot (\eta_i + 1)}$$

The total non-dimensional supporting force contributed by all pads underneath r-axis is then the sum of all components above:

$$W_{0\phi} = \sum_{i=2}^{N/2} W_{0\phi,i} + \lambda^2 \cdot W_{0\phi,1} \qquad (27)$$

$$W_{0r} = \sum_{i=2}^{N/2} W_{0r,i} + \lambda^2 \cdot W_{0r,1} \qquad (28)$$

Here λ is a number less than 1.0. In Figure-4, if the position of minimum film thickness is located within a pad, only a part of this pad will take load. The number "λ" is the percentage of the pad that takes load. The resultant force in dimensional form is then

$$W_0 = \frac{\mu \cdot V \cdot B^2 \cdot L}{c^2} \sqrt{W_{0\phi}^2 + W_{0r}^2} \qquad (29a)$$

The attitude angle:

$$\Phi = \tan^{-1} \frac{W_{0\phi}}{W_{0r}} \qquad (29b)$$

According to conventional definition of Sommerfeld Number for circular bearings, it is

$$S = \frac{\mu \cdot N_s \cdot d \cdot L}{W_0} \cdot \left(\frac{d}{2c}\right)^2 \tag{30}$$

The Sommerfeld Number for grooved bearings can be derived from equation (29a).

$$S = \frac{d^2}{4 \cdot \pi \cdot B^2 \cdot \sqrt{W_{0\phi}^2 + W_{0r}^2}} \tag{31}$$

d – Shaft Diameter

N_s - Shaft rotating speed in (rotation per second)

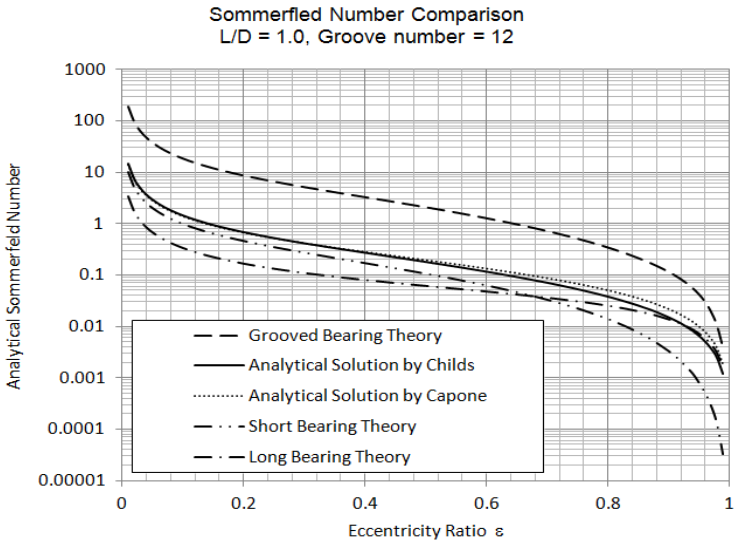

Figure-6: Sommerfeld Number Comparison

To verify the accuracy of Sommerfeld Number (31), several existing theories are put together with equation (31) for comparison. The available analytical equations are the short and long bearing theory, finite length bearing by Childs and Moes, and Capone, et al. From Figure-6, in comparison to non-grooved bearings, the grooved bearings have a significant lower load capacity. It is apparent that the water grooves have lowered the load capacity by reducing effective surface area and impairing the ability to form lubrication film. Among all the theoretical predictions for non-grooved plain bearings, Childs theory is considered to be most accurate. It meets the two criteria mentioned in introduction of this paper. Under given load condition, the Sommerfeld Number defined by equation (31) can be used to determine the eccentricity ratio and the minimum film thickness under steady operation.

The equilibrium position of shaft center under steady operation is the start point of analyzing the stiffness and damping as well as operational stability. The Sommerfeld Number for grooved bearing is significantly affected by number of grooves. Increased groove number causes a higher Sommerfeld Number, meaning a lower load capacity. This effect is demonstrated in Figure -7. In following discussion, the Sommerfeld Number by Childs and Moes [6] is considered to be accurate. In order to make a comparison, the ratio of the Sommerfeld Number of grooved bearing by equation (31) to the Sommerfeld Number by Childs and Moes is plotted in Figure -7.

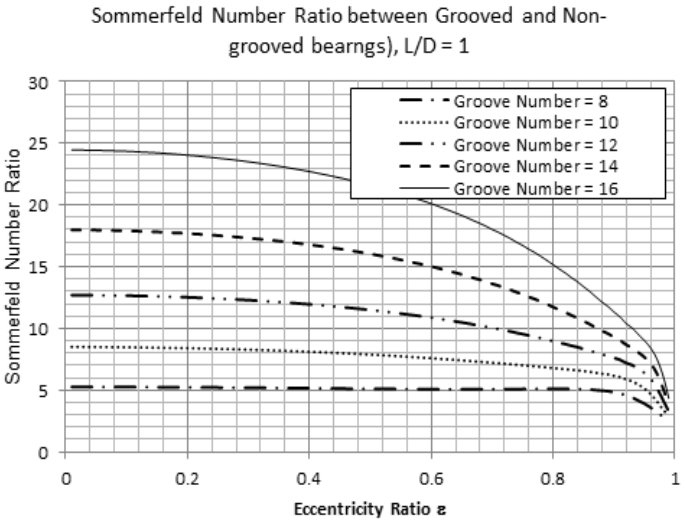

Figure -7: Effect of Groove Number on Sommerfeld Number Ratio

Figure -7 was created by assuming the L/D =1 for evaluating the non-grooved bearing by Childs and Moes. However, the Sommerfeld Number for grooved bearing is not changed with L/D ratio. As long as the L/B is great enough, the theory is considered to be valid. Figure-8 demonstrates the Sommerfeld Number ratio of grooved to non grooved bearings by changing L/D ratio.

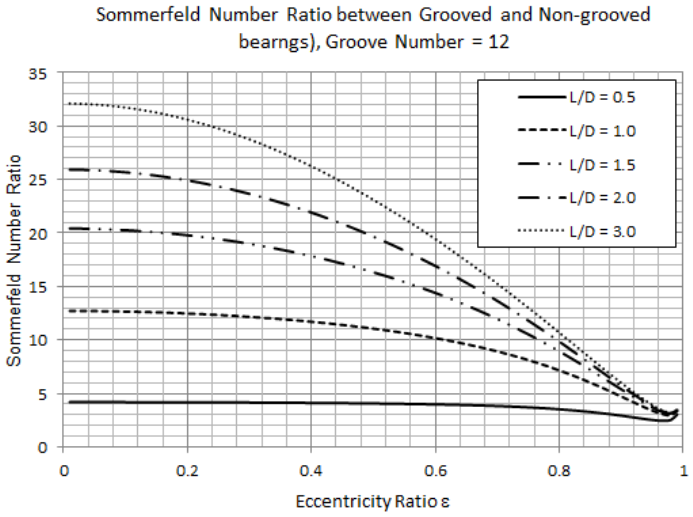

Figure-8, Effect of L/D on Sommerfeld Number ratio

Figure -8 is for groove number equal to 12. Water-lubricated guide bearings are usually designed at eccentricity ratio greater than 0.8 and L/D less than 1.0. In this range, the load capacity of grooved bearings might be 3 to 7 times lower than non-grooved bearings.

5. Stiffness and Damping Coefficients

Following the similar procedure in [2], the non-dimensional stiffness and damping coefficients for the entire bearing with multi-axial grooves are expressed as

$$K_{rr} = \sum_{i=2}^{N/2} \frac{\cos\alpha_{T,i}}{(1+\varepsilon\cdot\cos\alpha_{T,i})^3}\cdot K(\eta_i)\cdot\cos(\pi-\Theta_i) + \frac{\lambda^2\cdot\cos\alpha_{T,1}}{(1+\varepsilon\cdot\cos\alpha_{T,1})^3}\cdot K(\eta_1)\cdot\cos(\pi-\Theta_1)$$

$$K_{r\phi} = \sum_{i=2}^{N/2} \frac{\sin\alpha_{T,i}}{(1+\varepsilon\cdot\cos\alpha_{T,i})^3}\cdot K(\eta_i)\cdot\cos(\pi-\Theta_i) + \frac{\lambda^2\cdot\sin\alpha_{T,1}}{(1+\varepsilon\cdot\cos\alpha_{T,1})^3}\cdot K(\eta_1)\cdot\cos(\pi-\Theta_1)$$

$$K_{\phi r} = \sum_{i=2}^{N/2} \frac{\cos\alpha_{T,i}}{(1+\varepsilon\cdot\cos\alpha_{T,i})^3}\cdot K(\eta_i)\cdot\sin(\pi-\Theta_i) + \frac{\lambda^2\cdot\cos\alpha_{T,1}}{(1+\varepsilon\cdot\cos\alpha_{T,1})^3}\cdot K(\eta_1)\cdot\sin(\pi-\Theta_1)$$

$$K_{\phi\phi} = \sum_{i=2}^{N/2} \frac{\sin\alpha_{T,i}}{(1+\varepsilon\cdot\cos\alpha_{T,i})^3}\cdot K(\eta_i)\cdot\sin(\pi-\Theta_i) + \frac{\lambda^2\cdot\sin\alpha_{T,1}}{(1+\varepsilon\cdot\cos\alpha_{T,1})^3}\cdot K(\eta_1)\cdot\sin(\pi-\Theta_1) \quad (32)$$

$$C_{rr} = \sum_{i=2}^{N/2} \frac{C(\eta_i)}{(1+\varepsilon\cdot\cos\alpha_{T,i})^3}\cdot\cos^2(\pi-\Theta_i) + \frac{\lambda^3\cdot C(\eta_1)}{(1+\varepsilon\cdot\cos\alpha_{T,1})^3}\cdot\cos^2(\pi-\Theta_1)$$

$$C_{r\phi} = C_{\phi r} = \sum_{i=2}^{N/2} \frac{C(\eta_i)}{(1+\varepsilon\cdot\cos\alpha_{T,i})^3}\cdot\cos(\pi-\Theta_i)\cdot\sin(\pi-\Theta_i) + \frac{\lambda^3\cdot C(\eta_1)}{(1+\varepsilon\cdot\cos\alpha_{T,1})^3}\cdot\cos(\pi-\Theta_1)\cdot\sin(\pi-\Theta_1)$$

$$C_{\phi\phi} = \sum_{i=2}^{N/2} \frac{C(\eta_i)}{(1+\varepsilon\cdot\cos\alpha_{T,i})^3}\cdot\sin^2(\pi-\Theta_i) + \frac{\lambda^3\cdot C(\eta_1)}{(1+\varepsilon\cdot\cos\alpha_{T,1})^3}\cdot\sin^2(\pi-\Theta_1) \quad (33)$$

Translate them from r-ϕ coordinate frame into x-y coordinate frame, these are

$$\begin{bmatrix} KYY & KYX \\ KXY & KXX \end{bmatrix} = \begin{bmatrix} \cos\Phi & -\sin\Phi \\ \sin\Phi & \cos\Phi \end{bmatrix}\cdot\begin{bmatrix} K_{rr} & K_{r\phi} \\ K_{\phi r} & K_{\phi\phi} \end{bmatrix}\cdot\begin{bmatrix} \cos\Phi & \sin\Phi \\ -\sin\Phi & \cos\Phi \end{bmatrix} \quad (34)$$

$$\begin{bmatrix} CYY & CYX \\ CXY & CXX \end{bmatrix} = \begin{bmatrix} \cos\Phi & -\sin\Phi \\ \sin\Phi & \cos\Phi \end{bmatrix}\cdot\begin{bmatrix} C_{rr} & C_{r\phi} \\ C_{\phi r} & C_{\phi\phi} \end{bmatrix}\cdot\begin{bmatrix} \cos\Phi & \sin\Phi \\ -\sin\Phi & \cos\Phi \end{bmatrix} \quad (35)$$

The coefficients of stiffness KYY, KYX, KXY and KXX are non-dimensional. From equation group (32) and (33), it can be seen that they only depend on location angles and the number of grooves. This means they are changing with different groove configuration only. The same is applied to the damping coefficients. For purpose to make comparison with other available methods, here a new group of non-dimensional coefficients of stiffness and damping is defined as follows

$$\begin{aligned}
K_{yy} &= KYY\cdot\left(\frac{2B}{d}\right)^2\cdot S\cdot\pi \\
K_{yx} &= KYX\cdot\left(\frac{2B}{d}\right)^2\cdot S\cdot\pi \\
K_{xy} &= KXY\cdot\left(\frac{2B}{d}\right)^2\cdot S\cdot\pi \\
K_{xx} &= KXX\cdot\left(\frac{2B}{d}\right)^2\cdot S\cdot\pi \qquad (36)\\
C_{yy} &= CYY\cdot\left(\frac{2B}{d}\right)^3\cdot S\cdot\pi \\
C_{yx} &= CYX\cdot\left(\frac{2B}{d}\right)^3\cdot S\cdot\pi \\
C_{xy} &= CXY\cdot\left(\frac{2B}{d}\right)^3\cdot S\cdot\pi \\
C_{yy} &= CYY\cdot\left(\frac{2B}{d}\right)^3\cdot S\cdot\pi \qquad (37)
\end{aligned}$$

The Sommerfeld Number in above equations as defined in (31). It is a function of eccentricity ratio of bearing. The non-dimensional stiffness group in (36) and non-dimensional damping group in (37) is directly comparable with existing circular bearing results such as long and short bearing theory and others. In this paper, the stiffness and damping coefficients from Childs and Moes [6] are of particular interesting. They are considered to be accurate for non-grooved plain bearings and used for verifying the correctness of equation (36) and (37).

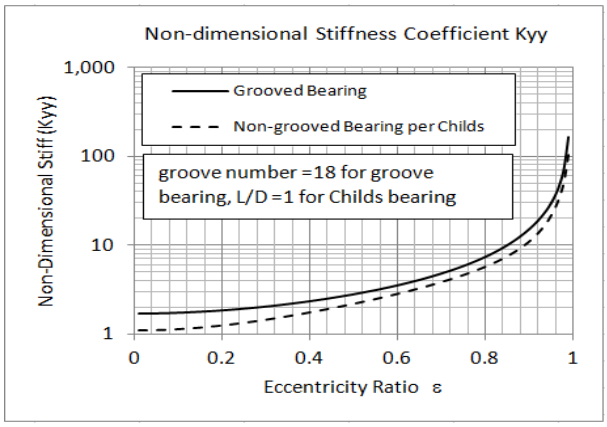

Figure-9-a

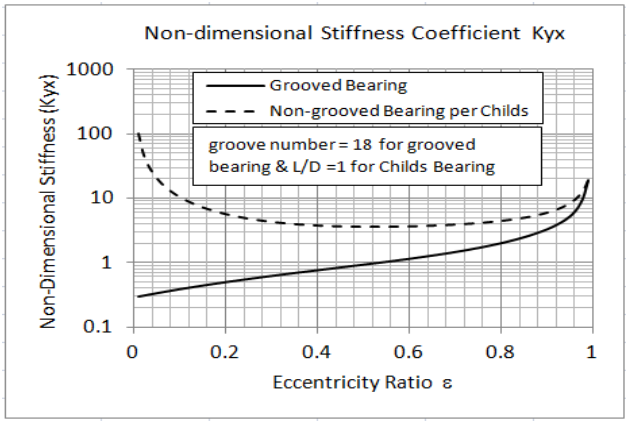

Figure-9-b

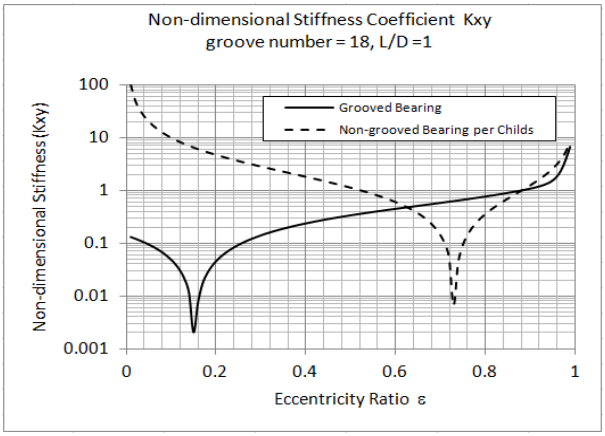

Figure -9-c

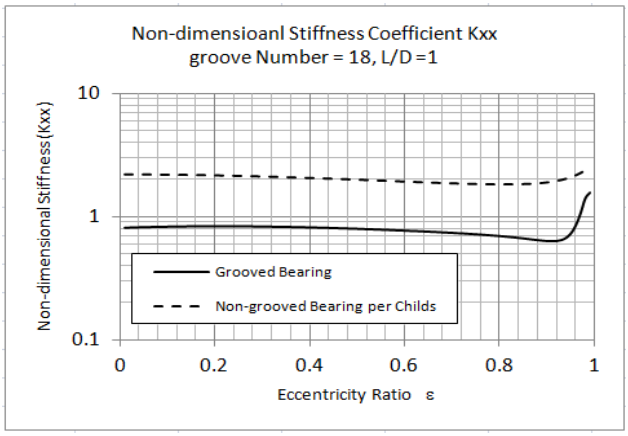

Figure-9-d

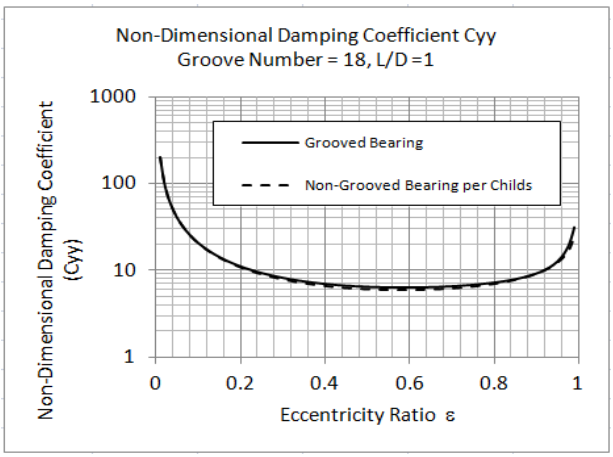

Figure -10-a

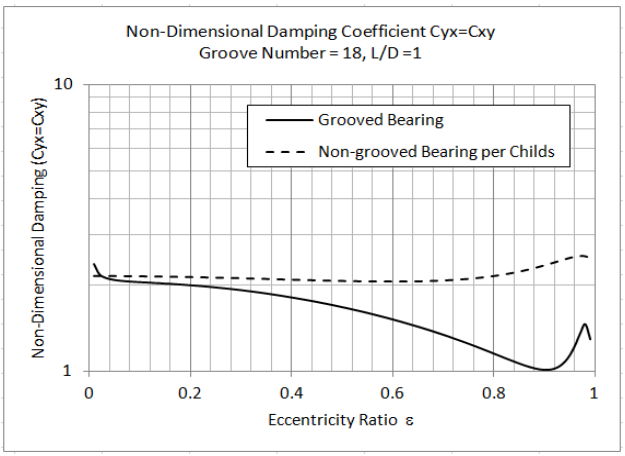

Figure -10-b

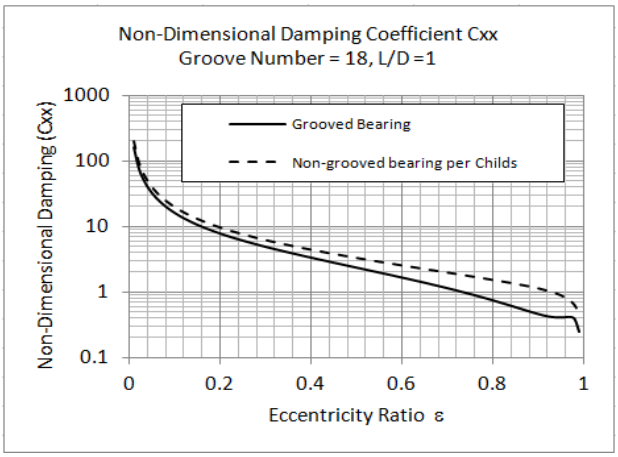

Figure-10-c

Same as for non-dimensional coefficients of stiffness, the coefficients of damping has also been compared at same groove number and L/D ratio. In Figure-9 and 10, the stiffness and damping coefficients by Childs and Moes was based on L/D = 1.0 and for grooved bearings was based on groove number = 18.

It is understandable that stiffness coefficient K_{yy} for grooved bearing is slightly greater than that for non-grooved bearing. This is because the pressure is more concentrated on the area around of loading center due to grooves. The same reason may explain why the coefficient of stiffness K_{xx} and K_{yx} of grooved bearing is smaller than that of non-grooved bearing. One of noticeable characteristic of the cross-stiffness coefficient K_{xy} is that the point turning into negative is shifted to lower eccentricity ratio. The damping coefficient C_{yy} is almost identical for both non-grooved bearing and grooved bearing in this particular geometrical condition. The coefficient C_{xx} of grooved bearing is lower than that of non-grooved bearing. The cross-damping coefficient $C_{xy} = C_{yx}$ has larger difference for high eccentricity ratio and small difference for low eccentricity ratio. Figure-9 and 10 demonstrates that calculation result with using the method introduced in this paper can have a sufficient accuracy for practice application.

6. Rotor Stability

A real shafting system of hydro turbines is a very complicated mass – elastic system in terms of rotor dynamic operation. However, the lowest critical frequency is still determined by the rigid body movement. For a simple rigid rotor, the critical mass [3] may be the most useful information for the design. According to [3], the non-dimensional critical mass is derived from stability criterion and expressed as

$$M_c = \frac{c \cdot m \cdot \Omega^2}{W_0} = \frac{C_{yy} \cdot K_{xx} + C_{xx} \cdot K_{yy} - (C_{yx} \cdot K_{xy} + C_{xy} \cdot K_{yx})}{C_{yy} + C_{xx}} \tag{38}$$

Where

M_c -Non-dimensional critical mass

c – Radial running clearance of guide bearing,

Ω - Shaft rotating speed,

m - Critical mass, a real mass bigger this critical mass will cause system instability

W_0 - Bearing force under steady operation

Since the critical mass is defined by the non-dimensional stiffness and damping, they are only depending on bearing geometry, not load and speed.

For vertical hydro turbines, the bearing load W_0 is different from rotor weight. With using equation (29), the non-dimensional critical mass can be correlated to Sommerfeld Number S. This is

$$M_{nc} = \frac{M_c}{\pi \cdot S} \tag{39}$$

The relation between the real dimensional critical mass and the non-dimensional critical mass defined in equation (39) is

$$M_{nc} = \frac{m \cdot \Omega}{\mu \cdot L} \cdot \left(\frac{cd}{d} \right)^3 \tag{40}$$

Where:

M_{nc} -New non-dimensional critical mass

cd – Diametrical running clearance

S – Sommerfeld Number by equation (31)

The new defined non-dimensional mass is also independent on bearing load and speed, but depends on groove design, namely, number of grooves and size and running. It is a very useful criterion for checking rotor stability during feasibility study of turbine shafting system, Figure-11.

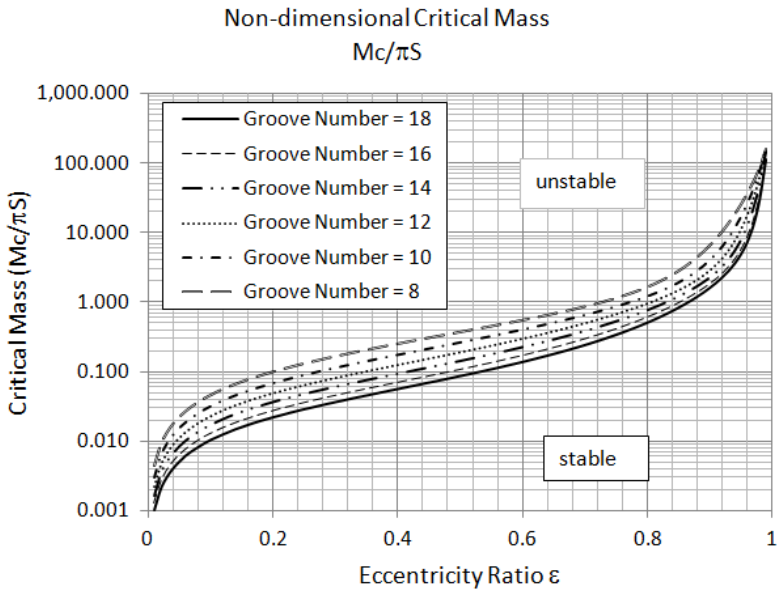

Fgiure-11: Non-dimension critical mass changed with groove number

7. Case study of a practice main guide bearing for a vertical turbine

This section shows one of real world turbine main guide bearing. The given design parameters were as following:

Shaft diameter:	1350 mm
Housing inside diameter:	1430 mm
Housing length:	1000 mm
Designed running clearance:	0.3 mm
Groove number:	18
Groove width:	10 mm
Normal load:	503 kN
Operation Speed:	50 rpm

Table-1 summarized results for two most loaded pads and minimum water film thickness under steady operational condition [2].

Table -1: Load on the most loaded pads and water film thickness (Pad numbering refers to Figure-4)

	Pad #1				Pad #2			
Load (kN)	λ=0.5		λ=1.0		λ=0.5		λ=1.0	
	110.5		393.5		349.5		98.69	
Percent %	21.5		76.5		68.1		19.2	
Water film Thickness at (μm)	Leading Edge	Trailing Edge	Leading Edge	Trailing Edge	Leading Edge	Trailing Edge	Leading Edge	Trailing Edge
	8.4	6.4	16.3	8.5	25.1	8.8	40.3	17.0

For a vertical turbine, the direction of load is undetermined. Therefore, calculation chose two extreme cases. λ =0.5 means the minimum film spot at 50% width of pad #1. λ=1 means the minimum film spot at trailing edge of pad #1.

Reference [2] has provided detail explanation about the condition for a hydrodynamic operation and the sufficiency of available film thickness. Steady operation evaluation provides further information about the equilibrium position of shaft. The stiffness and damping coefficients will be based on that position. Due to the large shaft diameter, this bearing has 18 grooves. Figure -12 is the non-dimensional stiffness coefficients and Figure -13 is the non-dimensional damping stiffness coefficients.

The physical dimensional coefficients of stiffness and damping are calculated at equilibrium position at which the eccentricity ratio = 0.956. The results calculated with grooved bearing theory are compared with traditional non-grooved bearing theory by Childs. All results are listed in table -2 below.

Table-2: Physical coefficients of stiffness and damping

	Stiffness Coefficients at ε = 0.956			Damping Coefficients at ε = 0.956	
	Grooved Bearing Theory (MN/mm)	Non-Grooved Theory by Childs and Moes (MN/mm)		Grooved Bearing Theory (MN-s/mm)	Non-Grooved Theory by Childs and Moes (MN-s/mm)
K_{yy}	113.430	87.164	C_{yy}	8.813	8.683
K_{yx}	19.429	30.078	C_{yx}	0.766	1.580
K_{xy}	5.725	8.538	C_{xy}	0.766	1.423
K_{xx}	2.700	6.652	C_{xx}	0.267	0.491
y – Axis is the loading direction; x-axis is perpendicular to load direction!					

For rotor stability, the non-dimensional critical mass defined by equation (39) can be used for a particular bearing design. This is

$$M_{nc} = \frac{M_c}{\pi \cdot S}$$

Figure -14 provides the critical rotor mass based on given shaft size and groove configuration. The actual critical mass based definition of equation (40) follows

$$M_A = \frac{m \cdot \Omega}{\mu \cdot L} \cdot \left(\frac{cd}{D}\right)^3$$

The stable condition is $M_A < M_{nc}$.

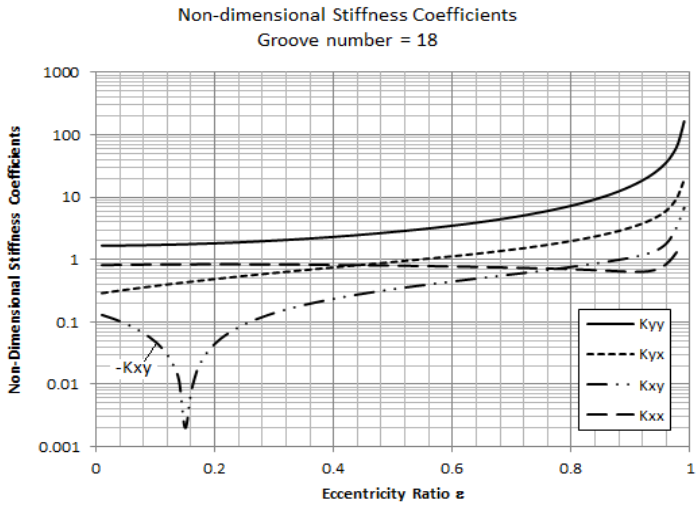

Figure-12, Non-dimensional stiffness for a bearing with 18 grooves

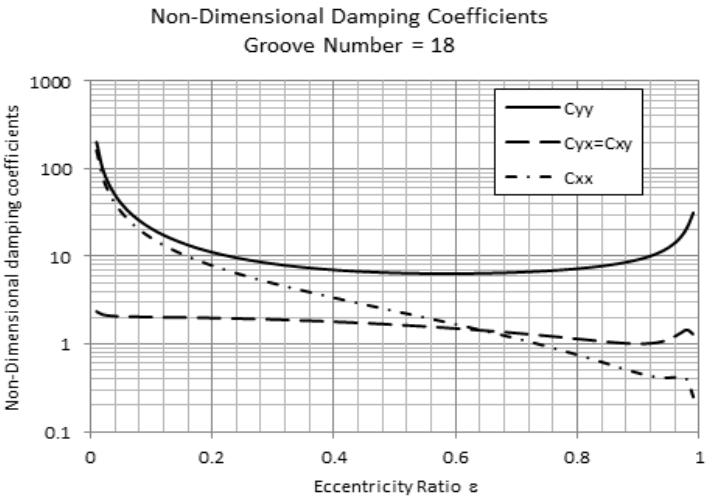

Figure -13: Non-Dimensional Damping Coefficients

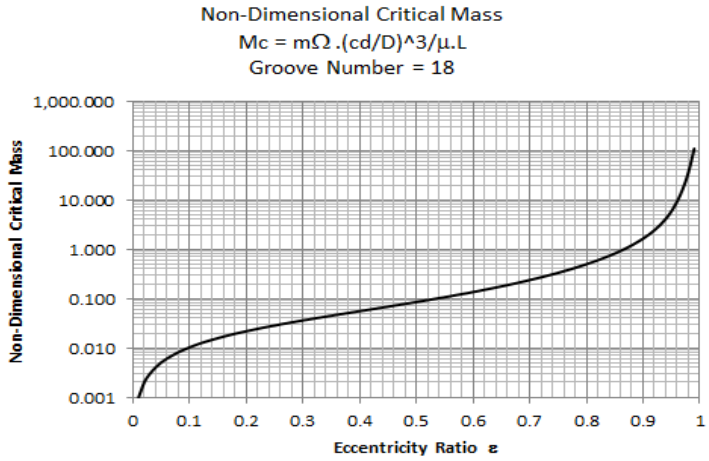

Figure -14: Non-Dimensional Critical Mass

8. Conclusion

This paper provides a new method to calculate the coefficients of stiffness and damping for water lubricated main guide bearings with multi-axial grooves for hydro turbines. The basic assumptions are the bearing surface is rigid, the bearing length to width of single pad ratio is larger than 3.0. The obtained result is compared with the existing method by Childs et al for non-grooved bearings.

First of all the paper concludes that the minimum thickness of the water film is thinner than a bearing without grooves under same load. This is as expected because water grooves reduce bearing surface and break down the continuity of water film. Secondly, the coefficient of stiffness in loading direction K_{yy} for grooved bearing is slightly higher than its counterpart of the non-grooved bearing under same eccentricity ratio. In other words, at same minimum water film thickness, the grooved bearing is slightly stiffer in loading direction than non-grooved one. This is because the pressure is more concentrated on the area around of loading center. The same reason also affects the coefficient of the cross-stiffness (K_{yx} K_{xy}) and lateral stiffness K_{xx}. The eccentricity ratio at which the stiffness component K_{xy} turns negative is generally believed a condition under that the bearing becomes instable. This study reveals that the eccentricity ratio at which K_{xy} turning negative is much lower for grooved bearing than for non-grooved bearing. This suggests a better stability of grooved bearing than non-grooved. Moreover, the new non-dimensional critical mass that incorporates Sommerfeld Number into it is only dependent on bearing geometry, meaning that they are only a function of bearing shaft diameter, bearing length, groove number and size, but not other physical parameter such as bearing load, shaft speed, water viscosity.

References:

1. Jaw-Ren Lin and Chi-Ren Hung, Analysis of dynamic characteristics for wide slider bearings with an exponential film profile, Journal of Marine Science and Technology, Vol. 12, No 3. pp 217-221, 2004
2. Guojun Ren, Calculation of Load Capacity and Water Film Thickness for Fully Grooved Water Lubricated Main Guide Bearings for Hydro Turbines, Hydro Vision Russia, Moscow, March 3-5, 2015
3. Mircea Rades: Dynamics of Machinery, II, Editura Printech, 2009, p99-102
4. Giancarlo Genta, Dynamics of Rotating Systems, ISBN 0-387-20936-0, 2005
5. Maurice L. Adams, Jr. Rotating Machinery Vibration From Analysis to Troubleshooting, ISBN: 0-8247-0258-1, 2001 Marcel Dekker, Inc.
6. D. Childs, H. Moes: H. Van Leeuwen: Journal Bearing Impedance Descriptions for Rotor dynamic applications, Transactions of ASME, p198, April, 1977
7. T. L. Daugherty, Frictional Characteristics of Water-Lubricated Compliant Surface Stave Bearings, ASLE, Transactions, Volume 24, 3, pp 293 – 301
8. Bernard J. Hanrock, Fundamentals of Fluid Film Lubrication, McGraw-Hill Inc. 1994
9. Virgiliu Niculae Constantinescu, Sliding Bearings, Allerton Press, Inc / New York, 1985
10. Andreas Z. Szeri, Fluid Film Lubrication, Theory and Design, Cambridge University Press, First Edition 1998
11. R.S. Pai and R. Pai, Stability of four-axial and six-axial grooved water-lubricated journal bearings under dynamic load, Proc. IMechE Vol. 222 Part J: J. Engineering Tribology, pp 683-691, 2008
12. Raimondi, A. A., and Boyd, J. (1958): A Solution for the Finite Journal Bearing and Its Application to Analysis and Design. ASLE Trans., vol. 1, pp. 159-209.
13. George B. DuBois and Fred W. Ocvirk, Analytical derivation and experimental evaluation of short-bearing approximation for full journal bearings, NACA report 1157
14. Lund, J.W. Spring and Damping Coefficients for the Tilting-Pad Journal Bearing, ASLE Trans., 7, 1964, pp 342-352
15. Nicholas, John C. Lund's Titling Pad Journal Bearing Pad Assembly Method, Transaction of ASME, vol.125, Oct 2003, pp 448 - 454
16. Lahmar, Mustapha; Ellagoune, Salah; Sou-Said, Benyebka, Elastohydrodynamic Lubrication Analysis of a Compliant Journal Bearing consiering static and dynamic deformations of the bearing liner, Tribology Transactions, 53, pp 349-368, 2010
17. G. Capone, V. Agostino, D. Guida, A finite Length Plain Journal Bearing Theory, Transaction of ASME, Vol. 116, July 1994, pp 648-653

The Authors

Guojun (Gary) Ren is a Chief Research Engineer. Gary worked as a senior mechanical engineer with ThyssenKrupp Elevator before joining Thordon bearings Inc. in 2001. Gary acquired his Ph.D. of mechanical engineering from University of Stuttgart in Germany in 1996. He is an expert on bearings, seals and rotor dynamics

Greg Auger is the Hydro Business Development Manager for Thordon Bearings Inc. Greg graduated from McMaster University in mechanical engineering in 2000 and joined Thordon Bearings Inc. as an Applications Engineer in 2007. He has extensive experience in the design, analysis, and installation of water lubricated bearings in Hydro turbines and Renewable energy applications.